Intraparticle Diffusion of 1-Phenyl-1, 2-ethanediol in Layered Double Hydroxides

Xiaolei Liu, Min Wei, Feng Li, and Xue Duan
State Key Laboratory of Chemical Resource Engineering, Beijing University of Chemical Technology, Beijing 100029, P.R. China

DOI 10.1002/aic.11184
Published online April 20, 2007 in Wiley InterScience (www.interscience.wiley.com).

The enantioselective adsorption of racemic 1-phenyl-1,2-ethanediol (PED) by carboxymethyl-β-cyclodextrin-intercalated Zn–Al- layered double hydroxides (CMCD-LDHs) has been studied. The adsorption isotherms of enantioselective as well as nonenantioselective adsorption of PED by CMCD-LDHs have been investigated, and it was found that the Langmuir–Frendlich and Frendlich model can be respectively used to describe the two different adsorptions satisfactorily. Furthermore, the intraparticle diffusion model is successfully validated in this work. Intraparticle effective diffusivities (D_{eff}) of PED in CMCD-LDHs macroparticle were determined from the homogeneous Fickian diffusion model, increasing with the increase of PED bulk phase concentration (C_0), which indicates the existence of parallel diffusion (crystallites diffusion and pore diffusion). The crystallites diffusivity (D_c) and pore diffusivity (D_p) for the parallel diffusion model were determined from the intercept and slope of the plot of $D_{eff}(1+1/\alpha)$ vs. $1/\alpha$, respectively. © 2007 American Institute of Chemical Engineers *AIChE J,* 53: 1591–1600, 2007
Keywords: LDHs, adsorption, parallel diffusion, pore diffusion, crystallites diffusion

Introduction

The study of enantioselective separation of chiral molecules with cyclodextrins (CDs) and chemically modified CDs has recently attracted much attention in the field of analytical and pharmaceutical research.[1–4] CDs are cyclic (α-1, 4)-linked oligosaccharides composed of α-D-glucopiranose with a hydrophilic outer surface and a relatively hydrophobic central cavity, which provides a microenvironment into which suitably sized lipophilic molecules may enter and be included.[5] CDs are usually used in capillary electrophoresis (CE) and chromatography for chiral recognition and chiral separation on the basis of the formation of transient diastereomers with the chiral centre of CDs and on the difference between their stability constants. Recently, studies dealing with immobilization of CDs have been reported for the application of ion uptake and separation, for instance, on the surface of hydroxylated silicas[6] and metals.[7,8]

Layered double hydroxides (LDHs), also known as hydrotalcite-like materials and anionic clays, which can be presented by the general formula $[M^{2+}_{1-x}M^{3+}_{x}(OH)_2]^{x+}$ $(A^{n-})_{x/n}\cdot mH_2O$, where M^{2+} and M^{3+} are di and trivalent metal cations, respectively. LDHs have positively charged layers and a wide variety of charge-balancing anionic species, A^{n-}, have been intercalated into the gallery region. As a result, these layered solids based upon the alternation of inorganic and organic layers have received considerable attention, because of their many practical applications, including as catalysts,[9] functional materials,[10] and nanocomposite materials.[11,12] The attractive feature of such materials is that they serve as a template for the formation of supramolecular structures.[13] The host layers can impose restricted geometry on the interlayer guests leading to enhanced control of stereochemistry, rates of reaction, and product distributions. Therefore the study of advanced materials based on LDHs is a rapidly growing field, and has application in areas such as separation science. The intercalation of chemically modified CDs into

Correspondence concerning this article should be addressed to X. Duan at duanx@mail.buct.edu.cn.

the galleries of LDH has been reported by Zhao[14] and Wang.[15] However, to the best our knowledge, enantioselective separation of racemates with CDs functionalized LDHs has not been previously reported.

In this study, the enantioselective adsorption of racemic PED by CMCD-LDHs has been investigated. PED is not only an important intermediate of chiral medicines and pesticides, but also a necessary chiral additive for liquid crystal material.[16–18] Compared with other adsorbents which have been used for chiral separation of PED, such as *trans*-1,2-cyclohexanediyl-bisacrylamide and cellulose triacetate,[19,20] CMCD-LDHs are easy and inexpensive to prepare and environmentally friendly. The adsorption isotherms of enantioselective as well as nonenantioselective adsorption of PED by CMCD-LDHs have been studied by using a batch method. Moreover, the parallel diffusion model is successfully validated in this work. Intraparticle effective diffusivities (D_{eff}) of PED in CMCD-LDHs macroparticle were determined from the homogeneous Fickian diffusion model, increasing with the increase of PED bulk phase concentration (C_0), which indicates the existence of parallel diffusion (crystallites diffusion and pore diffusion). The crystallites diffusivity (D_c) and pore diffusivity (D_p) for the parallel diffusion model were determined from the intercept and slope of the plot of $D_{\text{eff}}(1+1/\alpha)$ vs. $1/\alpha$, respectively. Therefore, a detailed understanding of the adsorption behavior of PED on CMCD functionalized LDHs should facilitate the application of such inorganic layered materials as chiral stationary phases for chromatographic columns.

Theory

Because of the strong electrostatic attraction between the LDHs layers and interlayer anions, we refer to the fact that a single LDHs macroparticle is an agglomerate of spherical crystallites, and the LDHs crystallites consist of LDHs layers and anions between the sheets. The adsorbate molecules diffuse into pores and are adsorbed on the crystallites walls, and also diffuse into the interlayer of LDHs crystallites and are adsorbed there. In order to simplify calculation, the LDHs crystallites are considered as microspheres, which can adsorb PED at the surface. Meanwhile, PED molecules can diffuse from one adsorption site to the next adsorption site, and also diffuse between the nearby crystallites. A macroparticle of LDHs is made up of lots of these crystallites microspheres (as shown in Figure 1).

In this experimental study, the intraparticle diffusion of PED in CMCD-LDHs was analyzed based on a parallel transport[21–28] by PED diffused in the crystallites (hereafter called crystallites diffusion) and the liquid-phase diffusion inside the network structure between crystallites (hereafter called pore diffusion). The following assumptions apply:

(1) Crystallites and pore diffusions occur in parallel inside the CMCD-LDHs macroparticles.

(2) Crystallites and pore diffusives are constant throughout the adsorption process.

(3) The void fraction of CMCD-LDHs macroparticle is constant throughout the adsorption process.

(4) The liquid-phase concentration of PED inside the particle is in local equilibrium with the concentration of the adsorbed PED in the LDHs crystallites.

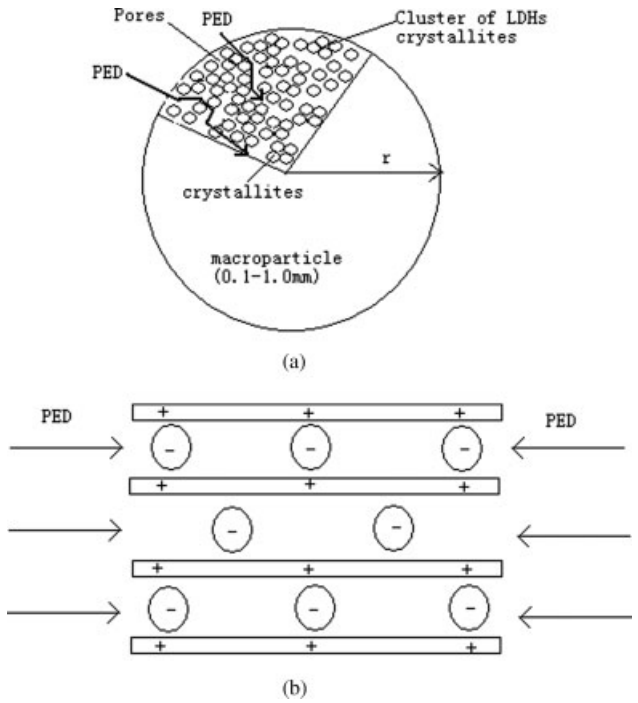

Figure 1. (a) Intraparticle diffusion of PED within a single LDHs macroparticle and (b) diffusion of PED in the crystallites of LDHs.

(5) The bulk phase concentration of PED is constant during the adsorption process.

The parallel diffusion model for this system can be written as follows:

$$\varepsilon\frac{\partial C}{\partial t}+(1-\varepsilon)\frac{\partial q}{\partial t}=D_{\text{p}}\varepsilon\frac{1}{r^2}\frac{\partial}{\partial r}\left(r^2\frac{\partial C}{\partial r}\right)+D_{\text{c}}(1-\varepsilon)\frac{1}{r^2}\frac{\partial}{\partial r}\left(r^2\frac{\partial q}{\partial r}\right) \quad (1)$$

where C (mol/m^3) represents liquid-phase concentration of PED inside the macroparticle, q (mol/m^3 wet LDHs) corresponds to solid-phase concentration of PED on the surface of the crystallites micropheres, r (m) is the radial dimension of an adsorbent particle, and ε denotes the void ratio of LDHs macroparticles. D_c and D_p (m^2/s) are the effective diffusivities in the crystallites and in the pore, respectively. Using the dimensionless variables, Eq. 1 is transformed into Eq. 2:

$$\frac{\partial X}{\partial \tau_p}+\alpha\frac{\partial Y}{\partial \tau_p}=\frac{1}{\xi^2}\frac{\partial}{\partial \xi}\left(\xi^2\frac{\partial X}{\partial \xi}\right)+\beta\frac{1}{\xi^2}\frac{\partial}{\partial \xi}\left(\xi^2\frac{\partial Y}{\partial \xi}\right) \quad (2)$$

where $X=C/C_{\text{e}}$, $Y=q/q_{\text{e}}$, $p=D_{\text{p}}t/r_0^2$, $\xi=r/r_0$, $\alpha=\frac{(1-\varepsilon)q_{\text{e}}}{\varepsilon C_{\text{e}}}$, $\beta=\frac{(1-\varepsilon)q_{\text{e}}D_{\text{c}}}{\varepsilon C_{\text{e}}D_{\text{p}}}=\alpha\frac{D_{\text{c}}}{D_{\text{p}}}$, and q_{e} (mol/m^3 wet LDHs) is the concentration of PED on the adsorption sites, in equilibrium with the concentration of PED in the bulk solution C_{e} (mol/m^3). r_0 (m) is radius of an adsorbent particle. The first and second terms of the right-hand side of Eq. 2 represent the contributions of pore diffusion and crystallites diffusion, respectively.

In this parallel diffusion model, α and β are the most important parameters. According to the definition, α means a

distribution coefficient, while β is the ratio of the rate of crystallites diffusion to that of pore diffusion. The degree of the contributions of crystallites and pore diffusions should be evaluated from the value of β. There are two limiting cases to consider here: when $\beta \to 0$ ($\varepsilon D_p C_e \gg (1-\varepsilon) D_c q_e$; pore diffusion control) and when $\beta \to \infty$ ($\varepsilon D_p C_e \ll (1-\varepsilon) D_c q_e$; crystallites diffusion control). When $\beta \to 0$, the second term on the right-hand side of Eq. 2 becomes zero and the equation for the pore diffusion control is obtained (Eq. 3). However, when $\beta \to \infty$, the second term of Eq. 2 becomes infinite consequently, the equation cannot be solved directly. Therefore, Eq. 1 is transformed into Eq. 4:

$$\frac{\partial X}{\partial \tau_p} + \alpha \frac{\partial Y}{\partial \tau_p} = \frac{1}{\xi^2} \frac{\partial}{\partial \xi} \left(\xi^2 \frac{\partial X}{\partial \xi} \right) \tag{3}$$

$$\frac{1}{\alpha} \frac{\partial X}{\partial \tau_c} + \frac{\partial Y}{\partial \tau_c} = \frac{1}{\xi^2} \frac{\partial}{\partial \xi} \left(\xi^2 \frac{\partial Y}{\partial \xi} \right) \tag{4}$$

When $\alpha \to \infty$, the concentration of PED adsorbed in the crystallites is substantially larger than that in the pore. In this case, pore diffusion is negligible and the crystallites diffusion is the rate-controlling step. This is confirmed by substituting $\alpha \to \infty$ into Eq. 2. Dividing both sides of Eq. 2 by α and using the definition of $\beta = (D_c/D_p)$, the terms related to the concentration of PED in the pore disappear and the following equation is obtained:

$$\frac{\partial Y}{\partial \tau_c} = \frac{1}{\xi^2} \frac{\partial}{\partial \xi} \left(\xi^2 \frac{\partial Y}{\partial \xi} \right) \quad \text{(crystallites diffusion control, } \alpha \to \infty) \tag{5}$$

When $\alpha \to 0$, the concentration of PED in the pore is much larger than in the crystallites. In this case, pore diffusion is the rate-controlling step, and the terms relate to the concentration in the crystallites disappear and the Eq. 6 is obtained:

$$\frac{\partial X}{\partial \tau_p} = \frac{1}{\xi^2} \frac{\partial}{\partial \xi} \left(\xi^2 \frac{\partial X}{\partial \xi} \right) \quad \text{(pore diffusion control, } \alpha \to 0) \tag{6}$$

Equilibrium as described by the equilibrium isotherms holds at the interface between the liquid and solid phases. In this case the model uses the Freundlich isotherm (Eq. 7):

$$q = kC^{1/n} \tag{7}$$

Using the dimensionless variables, Eq. 7 is transformed into Eq. 8

$$Y = k' X^{1/n}, \quad k' = \frac{k C_e^{1/n}}{q_e} \tag{8}$$

Using Eq. 8, Eq. 2 and Eq. 4 are transformed into Eq. 9 and Eq. 10, respectively, as follows:

$$\left\{ \alpha + \frac{n Y^{n-1}}{k'^n} \right\} \frac{\partial Y}{\partial \tau_p} = \frac{1}{\xi^2} \frac{\partial}{\partial \xi} \left\{ \xi^2 \frac{n Y^{n-1}}{k'^n} \frac{\partial Y}{\partial \xi} \right\} + \frac{\beta}{\xi^2} \frac{\partial}{\partial \xi} \left(\xi^2 \frac{\partial Y}{\partial \xi} \right) \tag{9}$$

$$\left\{ 1 + \frac{n Y^{n-1}}{\alpha k'^n} \right\} \frac{\partial Y}{\partial \tau_c} = \frac{1}{\xi^2} \frac{\partial}{\partial \xi} \left(\xi^2 \frac{\partial Y}{\partial \xi} \right) \tag{10}$$

As mentioned previously, Eq. 9 includes the expression of the pore diffusion control ($\beta = 0$). In addition, the following initial and boundary conditions apply:

$$\text{(IC)} \quad X = 0, \quad Y = 0 \quad \text{at} \quad \tau_p = 0 \quad \text{or} \quad \tau_c = 0 \tag{11}$$

$$\begin{aligned} \text{(BC)} \quad & \frac{\partial X}{\partial \xi} = 0, \quad \frac{\partial Y}{\partial \xi} = 0 \quad \text{at} \quad \xi = 0 \\ & X = 1, \quad Y = 1 \quad \text{at} \quad \xi = 1 \end{aligned} \tag{12}$$

Given that, only the change in the total concentration of PED in the particle Q_t (mol/m^3 wet LDHs), in Eq. 13, can be determined with time, while equilibrium adsorption capacity Q_e (mol/m^3 wet LDHs), in Eq. 14, can be obtained by adsorption at enough time.

$$Q_t = (1-\varepsilon) q + \varepsilon C = \frac{V(C_{a,0} - C_{a,t})}{V_{LDHs}} \tag{13}$$

$$Q_e = (1-\varepsilon) q_e + \varepsilon C_e = \frac{V(C_{a,0} - C_{a,e})}{V_{LDHs}} \tag{14}$$

where V and V_{LDHs} represent the solution volume and the wet LDHs volume. $C_{a,0}$, $C_{a,t}$, and $C_{a,e}$ represent the aqueous-phase PED concentration at initial, at time t, and at equilibrium, respectively.

Finally, the solution to the fractional attainment (F) of equilibrium under the initial and boundary conditions in Eqs. 11 and 12 is given by Eq. 15[29]:

$$\begin{aligned} F = \frac{Q_t}{Q_e} = \frac{3 \int_0^{r_0} Q_t r^2 dr}{r_0^3 Q_e} &= \frac{3 \left[\alpha \int_0^1 Y \xi^2 d\xi + \int_0^1 X \xi^2 d\xi \right]}{\alpha + 1} \\ &= 1 - \sum_{n=1}^{\infty} \frac{6\omega(\omega+1) \exp(-D_{eff} \lambda_n^2 t / r^2)}{9 + 9\omega + \lambda_n^2 \omega^2} \end{aligned} \tag{15}$$

where the λ_n values are the nonzero roots of

$$\tan \lambda_n = \frac{3\lambda_n}{3 + \omega \lambda_n^2} \tag{16}$$

and the parameter ω is expressed in terms of the final fractional uptake of solute by the LDHs macroparticles by the relation:

$$\frac{V_{LDHs} Q_e}{V C_{a,0}} = \frac{1}{1+\omega} \tag{17}$$

Experimental Section

Reagents

All chemicals including $Zn(NO_3)_2 \cdot 6H_2O$, $Al(NO_3)_3 \cdot 9H_2O$, NaOH, $NaNO_3$, methanol, chloroactic acid, β-CD, and (*R*,*S*)-PED were of analytical grade. β-CD was purchased from Aldrich, and the others from the Beijing Chemical Plant Limited.

Table 1. Experimental Physical Properties of CMCD-LDHs

Chemical Composition of MCD-LDHs	$Zn_{0.65}Al_{0.35}(OH)_2$ $(CMCD(3.8))_{0.037}$ $(CO_3)_{0.01}(NO_3)_{0.16}\cdot 0.9H_2O$
Particle diameter (m)	2.10×10^{-4}
True density (kg of dry CMCD-LDHs m^{-3})	1.88×10^{3}
Apparent density (kg of wet CMCD-LDHs m^{-3})	1.15×10^{3}
The void fraction of CMCD-LDHs macroparticles	0.327

Preparation and characterization

Synthesis of carboxymethyl-β-cyclodextrin, CMCD (3.8). CMCD (3.8) was synthesized according to the procedure described previously[30] and the average number of carboxylate groups per β-CMCD was calculated using ^{1}H NMR.[31]

Synthesis of CMCD-LDHs

The precursor $Zn_{0.67}Al_{0.33}(OH)_2(NO_3)_{0.33}$ (NO_3-LDHs) was synthesized by a procedure similar to that of described previously.[32,33] Under N_2 atmosphere through the conventional route, a solution of $Zn(NO_3)_2\cdot 6H_2O$ (1.2×10^{-1} M) and $Al(NO_3)_3\cdot 9H_2O$ (6.0×10^{-2} M) in deionized water (2.0×10^{-4} m^3) was added dropwise over 2 h to a solution of NaOH (3.1×10^{-1} M) and $NaNO_3$ (2.1×10^{-1} M) in water (1.0×10^{-4} m^3). The mixture was held at 343 K for 24 h. The precipitates were separated by centrifugation, washed with water, and dried at 343 K for 20 h.

The CMCD-LDHs was obtained by the method of ion exchange. A solution of CMCD (5.0×10^{-3} kg) in deionized water (5.0×10^{-5} m^3) was added to a suspension of NO_3-LDHs (1.0×10^{-2} kg) in water (1.0×10^{-4} m^3) and the solution pH was kept 6.0 by adding 1.0×10^2 mol/m^3 NaOH solution or 1.0×10^2 mol/m^3 HCl solution during reaction. The mixture was heated at 333 K under a nitrogen atmosphere for 48 h. The product was washed extensively with deionized water, centrifuged, and dried at 343 K for 20 h.

As Ca^{2+} cannot be adsorbed on LDHs layers, the void fraction of the CMCD-LDHs, ε, was obtained by dissolving the CMCD-LDHs whose pore was filled with $CaCl_2$ solution in HNO_3 solution (1.0×10^2 mol/m^3). The concentration of Ca^{2+} in the filtrate was determined by ICP. The value of ε was calculated according to Eq. 18, where C_{Ca} is the concentration of Ca^{2+} filled in the pore (mol/m^3); W and θ are the weight of the wet CMCD-LDHs particles (kg) and the apparent density (kg of wet CMCD-LDHs m^{-3}), respectively; $C_{f,Ca}$ and V_f are the concentration of PED in the filtrate (mol/m^3) and the volume of the filtrate (m^3), respectively. The experimental physical properties of CMCD-LDHs are listed in Table 1.

$$\varepsilon = \frac{C_{f,Ca}V_f}{(W/\theta)C_{Ca}} \tag{18}$$

Sorption experiments

PED sorption experiments were carried out using a batch method. Both the effects of contact time and PED concentration on the adsorption were investigated, the effect of contact time was used to determine kinetic model of PED sorption and equilibrium time. CMCD-LDHs (3.0×10^{-4} kg) and PED solutions (2.0×10^{-5} m^3) (typically ranging from 0.0 to 1.08×10^2 mol/m^3) were added to 5.0×10^{-5} m^3 Erlenmeyer stopper flasks. Subsequently, the flasks were capped, vigorously shaken by hand, were placed in a water bath at certain temperature (e.g. 303 K) and gently shaken for specific time period or until adsorption equilibrium. The suspensions were filtered, and the PED concentrations were determined at $\lambda = 256$ nm using UV–vis spectrophotometer. The amount of PED adsorbed by the CMCD-LDHs was calculated by the difference between the initial ($C_{a,0}$) and equilibrium concentrations ($C_{a,e}$), per kilogram of LDHs adsorbent: $Q_e = (C_{a,0} - C_{a,e}) \times V/m$.

Characterization

X-ray diffraction pattern of the samples were obtained using a Shimadzu XRD-6000 diffractometer with Cu-Kα radiation (40 kV and 30 mA) at a scanning rate of 5° min^{-1}. Elemental analysis was performed with a Shimadzu ICP-7500 instrument. The C, H, and N contents were determined using an Elementarvario elemental analysis instrument.

An UV–vis spectrophotometer (Shimadzu UV-2501PC) was used to measure the absorbance spectra of compounds in the 200–700 nm wavelength range. The concentration of PED in the solutions, before and after adsorption experiments, was determined using the UV–vis spectra at the wavelength of 256 nm.

Chiral HPLC (Daicel Chiralcel OB-H, 10% iPrOH in hexane, flow rate 0.5 ml/min) was used to determine e.e.% of the supernatants, by filtration after the adsorption experiment.

Experimental results

Characterization of NO_3-LDHs and CMCD-LDHs. The CMCD intercalated LDHs (CMCD-LDHs) was obtained by an anion-exchange process as described in the experimental part. Figure 2 displays the XRD patterns of the precursor NO_3-LDHs and the resulting composite. In each case, the reflections can be indexed to a hexagonal lattice with R-3m

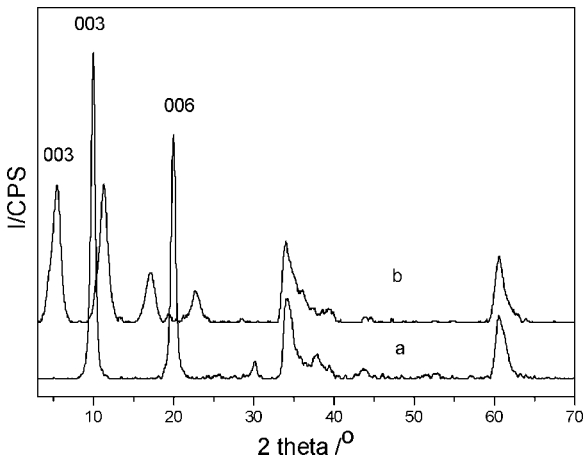

Figure 2. XRD patterns of (a) NO_3-LDHs and (b) CMCD-LDHs.

Table 2. Lattice Parameters of NO_3-LDHs and CMCD-LDHs

Lattice Parameter (nm)	NO_3-LDHs	CMCD-LDHs
d_{003}	0.889	1.641
d_{006}	0.445	0.819
d_{009}	0.297	0.518
d_{110}	0.152	0.152
Lattice parameter a	0.304	0.304
Lattice parameter c	2.667	4.923

rhombohedral symmetry, commonly used for the description of LDHs structures. The basal spacing and lattice parameters are listed in Table 2. The Zn/Al-NO_3 LDHs precursor has an XRD pattern similar to that reported previously,[32] with an interlayer spacing (d_{003}) of 0.889 nm. After intercalation of CMCD, the interlayer distance increased to 1.641 nm. The expanded interlayer separation is consistent with the intercalation of the organic anions within the gallery spaces of the LDHs. Since the thickness of the LDHs hydroxide basal layer is 0.480 nm, the gallery height is 1.161 nm.

As shown in Figure 2b, the intensity of (006) reflection of CMCD-LDHs is almost the same as that of (003) while the (003) reflection has the strongest peak intensity in the diffraction pattern of the LDHs precursor. This is possibly related to the presence of a CO_3-LDH impurity phase that is often observed even when intercalation reactions are carried out under nitrogen. The peak around $2\theta=11^\circ$ may be a superposition of the (003) reflection of CO_3-LDH and the (006) reflection of the CMCD-LDHs, accounting for its enhanced intensity. The peak around $2\theta = 23^\circ$ can be assigned to the (006) reflection of CO_3-LDH.

CD should be regarded as truncated cone rather than a cylinder. There are 7 primary and 14 secondary hydroxyl groups along the β-CD cavity. β-CD has an approximate torus thickness of 0.78 nm, and outer diameter of 1.53 nm, and an inner diameter of 0.78 nm.[34] Taking into account the dimensions of the β-CD molecule and the rule of charge balance, the CMCD (3.8) anions can only adopt a monolayer arrangement with its cavity axis perpendicular to the LDHs layer and carboxymethyl groups on adjacent CD molecules attached alternately to the upper and lower LDHs layer surfaces. This is similar to the arrangement reported by Zhao and Vance[14] for CMCD interlayered into Mg/Al-LDH.

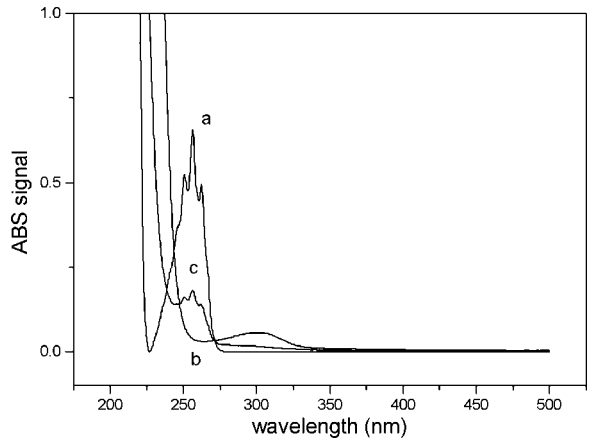

Figure 3. UV–vis spectra of (a) PED, (b) CMCD-LDHs, and (c) adsorption product of CMCD-LDHs.

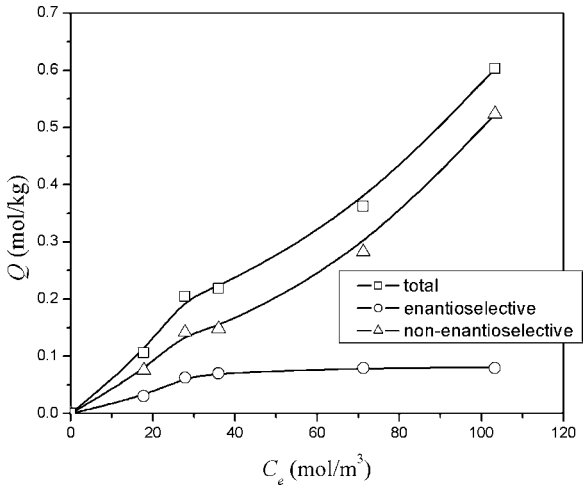

Figure 4. The total, enantioselective, and nonenantioselective adsorption isotherms of PED by CMCD-LDHs at 303 K.

Adsorption equilibrium

The UV–vis spectra of CMCD-LDHs before and after the adsorption of PED are shown in Figure 3. Compared with the as-synthesized CMCD-LDHs (Figure 3b), the spectrum of the adsorption product shows three strong bands at 265, 256, and 251 nm (Figure 3c), respectively, which is in accordance with the characteristic of the pristine PED (Figure 3a). This indicates the occurrence of the adsorption of PED on CMCD-LDHs.

Chiral HPLC (Daicel Chiralcel OB-H, 10% *i*PrOH in hexane, flow rate 0.5 ml/min) was used to determine e.e.% of the supernatants, by filtration after the adsorption experiment.

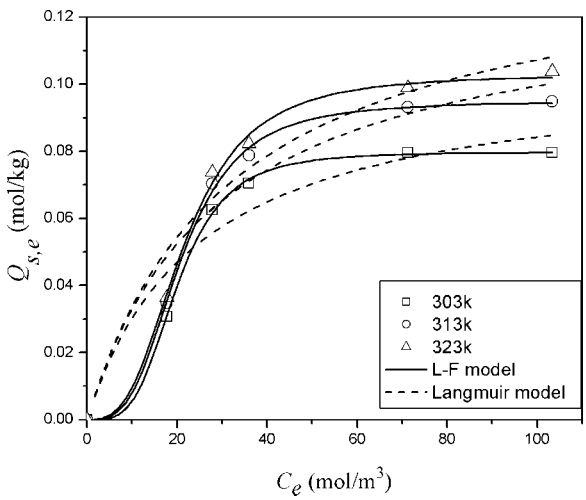

Figure 5. The enantioselective adsorption isotherms of R-PED by CMCD-LDHs fitted by Langmuir and L–F model at 303, 313, and 323 K, respectively.

Table 3. Langmuir and L–F Constants for the Enantioelective Adsorption of R-PED by CMCD-LDHs at Different Temperatures

	Langmuir Model			L–F Model			
Temp. (K)	K_L (m^3/kg)	Q_m (mol/ kg)	R^2	K_L (m^3/kg)	Q_m (mol/kg)	N	R^2
303	3.82×10^{-2}	2.37×10^{-1}	0.915	3.80×10^{-4}	8.12×10^{-2}	5.09	0.995
313	2.27×10^{-2}	5.26×10^{-1}	0.908	1.48×10^{-4}	9.52×10^{-2}	4.16	0.989
323	1.11×10^{-2}	1.29	0.914	3.92×10^{-3}	1.04×10^{-1}	3.37	0.994

The results indicate that *R*-PED was adsorbed preferentially by CMCD-LDHs (see Supplementary Material). It can be speculated that the adsorption of PED by CMCD-LDHs includes two parts: the enantioselective adsorption (Q_s) resulting from the chiral reorganization of interlayer immobilized CMCD and the nonenantioselective adsorption ($Q_{non\text{-}s}$) produced by the surface of LDHs layers, which can be calculated by

$$Q_s = C_{a,t} \times V \times \text{e.e.}\%/m \tag{19}$$

$$Q_{non-s} = \frac{(C_{a,0} - C_{a,t}) \times V - C_{a,t} \times V \times \text{e.e.}\%}{m} \tag{20}$$

Thus the adsorption isotherms, including enantioselective and nonenantioselective adsorption, were plotted (Figure 4).

As for the enantioselective adsorption of PED by CMCD-LDHs, two models were used to fit the experimental data: (1) Langmuir model (Eq. 21);[35,36](2) Langmuir–Frendlich (L–F) model (Eq. 22)[37]

$$\frac{Q_e}{Q_m} = \frac{K_L C_{a,e}}{1 + K_L C_{a,e}} \tag{21}$$

$$\frac{Q_e}{Q_m} = \frac{K_L C_{a,e}^n}{1 + K_L C_{a,e}^n} \tag{22}$$

where $C_{a,e}$ is the equilibrium concentration of PED in the solution (mol/m^3); Q_e is the adsorption capacity at equilibrium (mol/kg); Q_m and K_L are the Langmuir constants related to the capacity and energy of adsorption, respectively, and n is also a model parameter. According to the classification of Giles et al.[38] although the enantioselective adsorption by CMCD has a maximum adsorption capacity, the shape of its isotherm cannot be considered simply as pure L-type. Figure 5 displays the enantioselective adsorption isotherms of PED by CMCD-LDHs at different temperatures, fitted by Langmuir and L–F model, respectively. The experimental conditions, the estimated model parameters and regress coefficients (R^2) are reported in Table 3 for all enantioselective adsorption experimental runs.

As can be seen from Table 3, the regress coefficients (R^2) for the L–F model are larger than that for Langmuir model, and the experimental $Q_{s,e}$ values agree well with the calculated ones obtained from L–F model. This indicates that the L–F model can be used to describe the enantioselective adsorption of PED by CMCD-LDHs satisfactorily.

Figures 6 and 7 display the nonenantioselective and total adsorption isotherms at 303, 313, and 323 K, respectively. Owing to the shape of the isotherms, the nonenantioselective, and total surface sorption data were analyzed according to Freundlich equation[36]:

$$Q_e = K C_{a,e}^{1/n} \tag{23}$$

where Q_e is the amount of PED per unit weight of the LDHs; $C_{a,e}$ is the equilibrium concentration of PED in the solution (mol/m^3); K and n are Freundlich temperature-de-

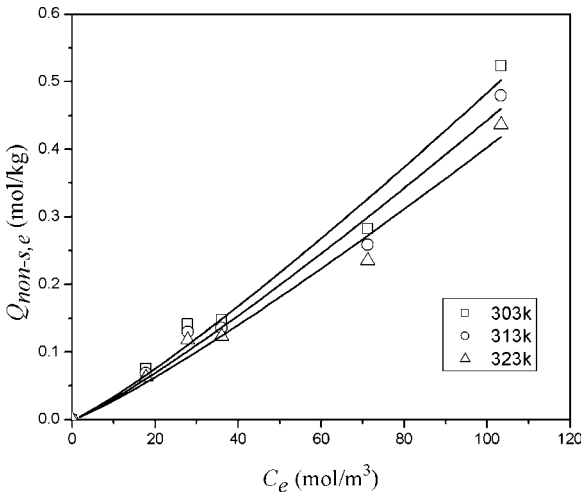

Figure 6. The nonenantioselective adsorption isotherms of (*R*,*S*)-PED by CMCD-LDHs at 303, 313, and 323 K, respectively.

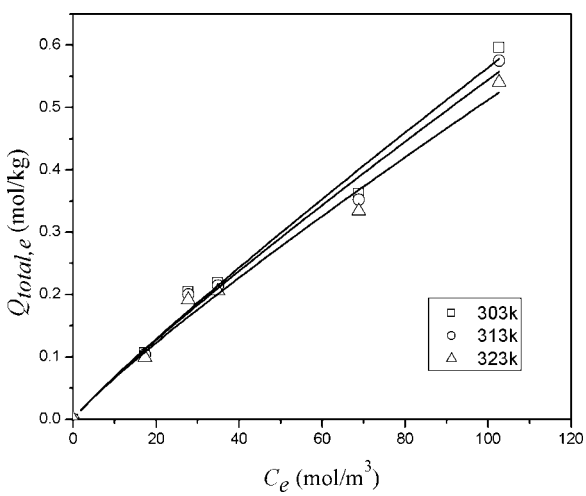

Figure 7. The total adsorption isotherms of (*R*,*S*)-PED by CMCD-LDHs at 303, 313, and 323 K, respectively.

Table 4. Freundlich Constants for the Nonenantioselective and Total Adsorption of (*R*,*S*)-PED by CMCD-LDHs at Different Temperatures

Temp. (K)	Nonenantioselective			Total		
	K	n	R^2	K	n	R^2
303	2.38×10^{-3}	0.867	0.983	8.27×10^{-3}	1.09	0.981
313	2.19×10^{-3}	0.867	0.990	8.53×10^{-3}	1.11	0.981
323	1.99×10^{-3}	0.869	0.987	8.65×10^{-3}	1.13	0.980

pendent constants. Table 4 lists the Freundlich constants for the nonenantioselective and total adsorption at different temperatures. The experimental $Q_{\text{non-s,e}}$ values and $Q_{\text{total,e}}$ agree well with the calculated ones obtained from Freundlich model, indicating that both the nonenantioselective and total adsorption isotherms can best be represented by the Freundlich model.

Study on the diffusion kinetics

Intraparticle effective diffusivity. To determine the crystallites diffusivity D_c (m^2/s) and the pore diffusivity D_p (m^2/s) based on the parallel diffusion model, the intraparticle effective diffusivity D_{eff} (m^2/s) at 303, 313, and 323 K for the homogeneous model was calculated. Assuming Fickian diffusion with a constant intraparticle effective diffusivity, the mass balance equation over the particle is given by the following equation:

$$\frac{\partial Q}{\partial t} = D_{\text{eff}} \frac{1}{r^2} \frac{\partial}{\partial r} \left(r^2 \frac{\partial Q}{\partial r} \right) \tag{24}$$

The initial (IC) and boundary conditions (BC) are given as follows:

$$\text{(IC)} \quad Q = 0 \quad \text{at} \quad t = 0 \tag{25}$$

$$\text{(BC)} \quad \frac{\partial Q}{\partial r} = 0 \quad \text{at} \quad r = 0 \qquad Q = Q_e \quad at \quad r = r_0 \tag{26}$$

In the adsorption experiments, the change of bulk concentration before and after adsorption is about 7%, as a result the bulk concentration can be considered to be constant approximately during the adsorption process. This gives the above boundary condition at the surface of the adsorbent particle, i.e., the adsorbent-phase concentration at the surface of the particle is constant.

The value of the intraparticle effective diffusivity (D_{eff}) was determined by fitting the experimental adsorption data with Eq. 15.

Initializing different values of D_{eff} until the best fit was obtained. As shown in Figure 8, the experimental values were well correlated by Eq. 15. The experimental values of D_{eff} are listed in Table 5. D_{eff} increased with increasing bulk-phase PED concentration, indicating an existence of a parallel transport by both crystallites and pore diffusions in the LDHs macroparticles.

Crystallites diffusivity and pore diffusivity

The relationship between crystallites diffusivity, pore diffusivity, and intraparticle effective diffusivity based on parallel diffusion model is given by the following equation, which is derived from the relation between the fluxes based on the parallel diffusion model and the Fickian model:

$$D_{\text{eff}} \left[(1 - \varepsilon) + \varepsilon \frac{dC}{dq} \right] = (1 - \varepsilon) D_c + \varepsilon D_p \frac{dC}{dq} \tag{27}$$

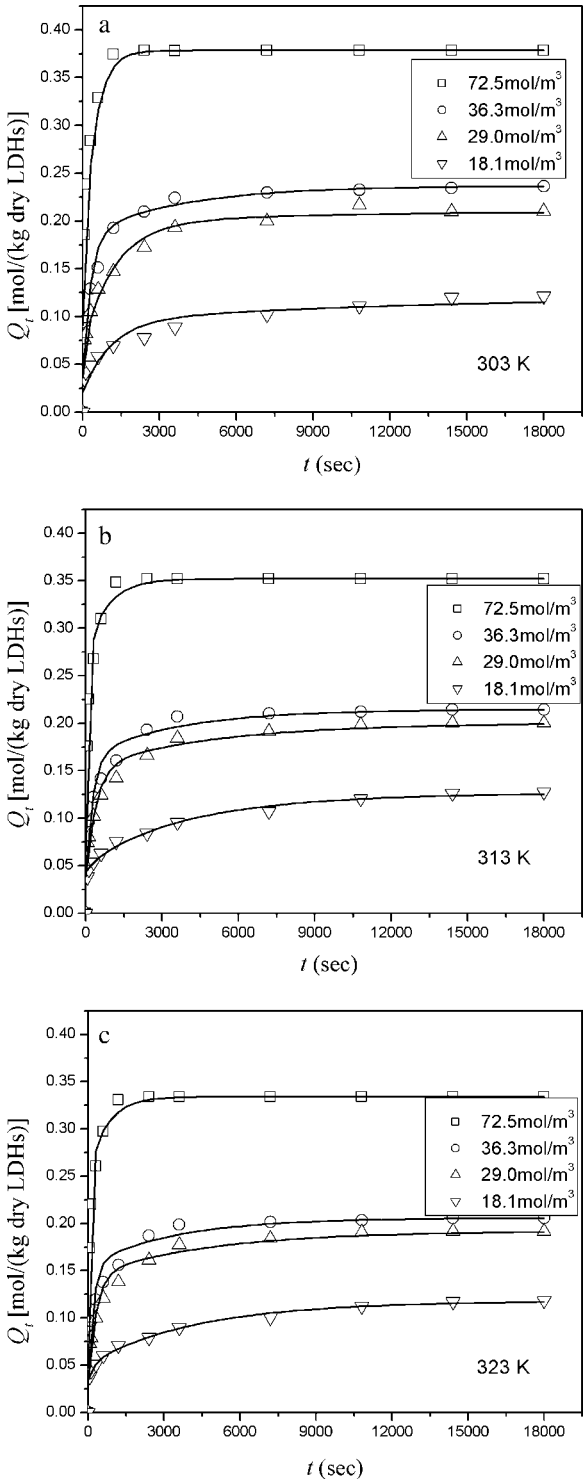

Figure 8. Effect of concentration on the uptake curves for adsorption of PED on CMCD-LDHs at (a) 303 K, (b) 313 K, and (c) 323 K, respectively.

Table 5. Determined Parameters against Initial Concentration

Temp. (K)	$C_{a,0}$ (mol/m^3)	D_{eff} (10^{12} m^2/s)	D_c (10^{12} m^2/s)	D_p (10^{11} m^2/s)	α	β
303	72.5	7.67	1.46	6.65	9.69	0.213
	36.3	6.21			12.1	0.266
	29.0	5.83			13.5	0.297
	18.1	5.40			16.3	0.359
313	72.5	7.79	1.53	6.84	9.62	0.212
	36.3	6.93			11.6	0.256
	29.0	6.07			13.5	0.298
	18.1	5.91			14.3	0.316
323	72.5	8.49	1.58	7.05	9.08	0.199
	36.3	7.18			11.0	0.242
	29.0	6.52			12.9	0.283
	18.1	6.37			13.7	0.292

Since, in our experimental method, the adsorption isotherm could be considered linear in the concentration range examined. By taking $dC/dq = C_e/q_e$ as an approximation, Eq. 27 is transformed into Eq. 28:

$$D_{eff}\left(1+\frac{1}{\alpha}\right) = D_c + D_p\frac{1}{\alpha} \tag{28}$$

Figure 9 shows the plot of the experimental effective diffusivities based on Eq. 28 at 303, 313, and 323 K, respectively. The value of the intercept of the line gives the crystallites diffusivity D_c and the slope of the line provides the pore diffusivity D_p, which are listed in Table 5. It can be seen that the values of D_{eff}, D_c, and D_p increase continuously with temperature from 303 to 323 K, indicating that higher temperatures favor diffusion of PED in LDHs.

Parallel transport by crystallites and pore diffusion

The theoretical adsorption curves for PED in CMCD-LDHs were calculated based on the parallel transport by crystallites and pore diffusions, given in Eq. 2, using the experimental values of crystallites diffusivity (D_c), pore diffusivity (D_p), and the dimensionless parameters in Table 5.

Figure 10 shows the experimental and theoretical uptake curves for adsorption of PED by CMCD-LDHs with different PED concentrations at 303 K. The solid lines are the theoretical ones determined from Eq. 2, which correlated reasonably well with the experimental adsorption data. The theoretical lines for the crystallites diffusion control and the pore diffusion control were likewise calculated, represented by broken and chain lines, respectively. The theoretical lines for the

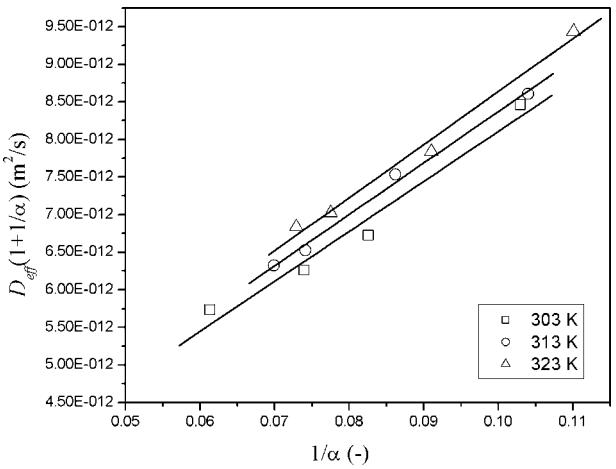

Figure 9. Plots of intraparticle effective diffusivities based on Eq. 28.

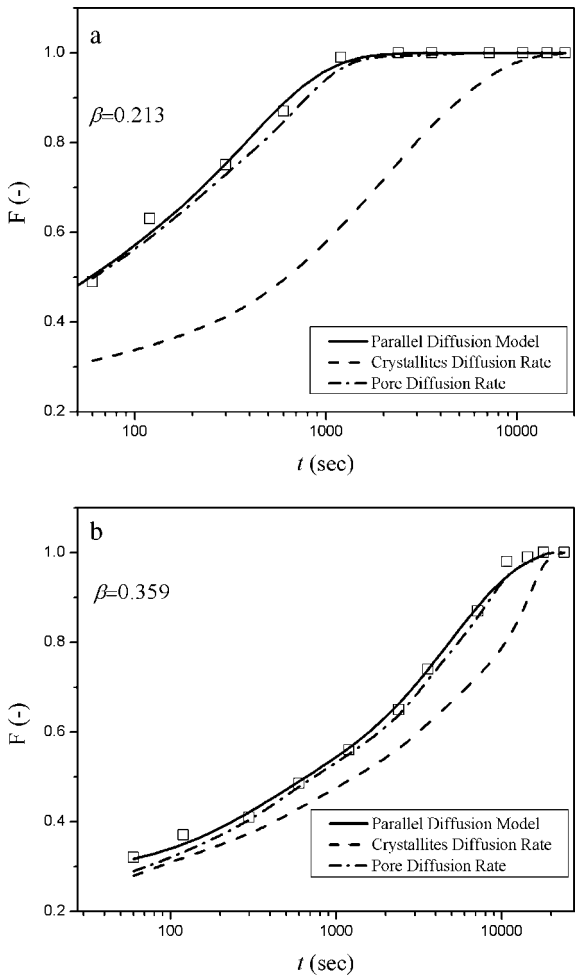

Figure 10. Experimental and theoretical uptake curves for the adsorption of PED by CMCD-LDHs for (a) C_0 = 72.5 mol/m^3 and (b) C_0 = 18.1 mol/m^3, respectively.

crystallites diffusion control were obtained by setting $1/\alpha = 0$ (see Eq. 5) and using the experimental values of D_c in Table 5. However, pore diffusion is the rate-controlling step, when $\beta = 0$ ($D_c = 0$), and thus the theoretical lines for the pore diffusion control were determined based on Eq. 3 and using the experimental values of D_p in Table 5.

In Figure 10, the adsorption data are very close to the theoretical lines of the pore diffusion control model (chain line) and significantly deviated from the crystallites diffusion control model (broken line). This indicates that only the contribution of pore diffusion is significant in this system. As mentioned earlier in the theoretical section, there are two limiting cases to be considered: $\beta \rightarrow 0$ (pore diffusion control) and $\beta \rightarrow \infty$ (crystallites diffusion control). When $\beta < 0.4$ (Table 5), it can be assumed that pore diffusion is the rate-controlling step. The results are consistent with the work conducted by Yoshida et al.[21] in the study of Phosphates adsorbed by an OH-type strongly basic ion exchanger, DIAION SA10A.

Conclusions

The CMCD-LDHs has been demonstrated to represent enantioselective adsorption for (*R*,*S*)-1-phenyl-1, 2-ethanediol, which suggests that this CMCD functionalized inorganic layered material may have prospective application as the basis of a novel chiral separation system. The adsorption isotherms of enantioselective as well as nonenantioselective adsorption of PED by CMCD-LDHs have been investigated, and it was found that the L–F and Frendlich model could be respectively used to describe the two different adsorptions satisfactorily. Moreover, the parallel transport of PED by crystallites and pore diffusion in CMCD-LDHs macroparticle was investigated. The values of the intraparticle effective diffusivity (D_{eff}) obtained from the homogeneous Fickian model increased with increasing bulk phase concentration for the whole rang of PED concentration. The crystallites (D_c) and pore (D_p) diffusivities were determined from the intercept and slope of the plot of $D_{eff}(1+1/\alpha)$ vs. $1/\alpha$, respectively. The parallel diffusion model is successfully validated in this work. The theoretical lines of the parallel diffusion model using D_c and D_p agreed well with the experimental data, and the contribution of pore diffusion is significant in this system.

Acknowledgments

This project was supported by the National Natural Science Foundation Major International Joint Research Program (Project No.: 20620130108), National Natural Science Foundation of China (Grant No.: 20601001), the Program for New Century Excellent Talents in University (Project No.: NCET-05-121) and the 111 Project (Project No.: B07004).

Notation

C = liquid-phase concentration of PED inside the macroparticle (mol/m^3)
$C_{a,0}$ = initial aqueous-phase PED concentration (mol/m^3)
$C_{a,t}$ = aqueous-phase PED concentration at time t (mol/m^3)
$C_{a,e}$ = aqueous-phase PED concentration at equilibrium (mol/m^3)
C_{Ca} = the concentration of Ca^{2+} filled in the pore (mol/m^3)
C_e = the equilibrium concentration of PED in the pore (mol/m^3)
$C_{f,Ca}$ = the concentrate of Ca^{2+} in the filtrate (mol/m^3)
D_{eff} = intraparticle effective diffusivity (m^2/s)
D_p = pore diffusivity (m^2/s)
D_c = the effective diffusivity in the crystallites (m^2/s)
F = fractional attainment of equilibrium
K_L = Langmuir equilibrium constant (m^3/mol)
m = the mass of CMCD-LDHs (kg)
q = solid-phase concentration of PED on the surface of the crystallites microperes (mol/m^3)
q_e = the equilibrium concentration of PED on the adsorption sites (mol/m^3)
Q_e = the adsorption capacity at equilibrium (mol/kg)
Q_t = $((1-\varepsilon)q+\varepsilon C)$ total concentration of PED in the particle (mol/m^3) wet LDHs
$Q_{s,e}$ = the enantioselectively sorption capacity at equilibrium (mol/kg)
$Q_{non\text{-}s,e}$ = the nonenantioselectively sorption capacity at equilibrium (mol/kg)
$Q_{total,e}$ = the total sorption capacity at equilibrium (mol/kg)
Q_e = $((1-\varepsilon)q_e+\varepsilon C_e)$ total concentration of PED in the particle in equilibrium (mol/m^3) wet LDHs
r = radial dimension of an adsorbent particle (m)
r_0 = radius of an adsorbent particle (m)
t = time (s)
V_f = the volume of the fitrate (m^3)
W = weight of the wet CMCD-LDHs particles (kg)
X = (C/C_e) dimensionless constant
Y = (q/q_e)) dimensionless constant

Greek letters

α = $(1-\varepsilon)q_e/\varepsilon C_e$
β = $\alpha(D_c/D_p)$
ε = void ration of LDHs macroparticles
λ_n = the nonzero roots of Eq. 16
ξ = r/r_0
ω = final fractional uptake of solute by the LDHs macroparticles
τ_p = $D_p t/r_0^2$
τ_c = $D_c t/r_0^2$
θ = the apparent density, kg of wet CMCD-LDHs (m^{-3})

Literature Cited

1. Lipkowitz KB, Coner R, Peterson MA. Locating regions of maximum chiral discrimination: a computational study of enantioselection on a popular chiral stationary phase used in chromatography. *J Am Chem Soc*. 1997;119:11269–11276.
2. Liu Y, Li B, Han BH, Li YM, Chen RT. Enantioselective recognition of amino acids by β-cyclodextrin 6-*O*-monophosphates. *J Chem Soc, Perkin Trans II*. 1997;997:1275–1278.
3. Rekharsky MV, Inoue Y. Complexation and chiral recognition thermodynamics of 6-amino-6-deoxy-β-cyclodextrin with anionic, cationic, and neutral chiral guests: counterbalance between van der Walls and Coulombic interactions. *J Am Chem Soc*. 2002;124:813–826.
4. Xu YF, McCarroll ME. Fluorescence anisotropy as a method to exanine the thermodynamics of enantioselectivity. *J Phys Chem B*. 2005;109:8144–8152.
5. Faucci MT, Melani F, Mura P. Computer-aided molecular modeling techniques for predicting the stability of drug-cyclodextrin inclusion complexes in aqueous solutions. *Chem Phys Lett*. 2002;358:383–390.
6. Belyakov VN, Belyakova LA, Varvarin AM, Khora OV, Vasilyuk SL, Kazdobin KA, Maltseva TV, Kotvitskyy AG, Danil de Namor AF. Supramolecular structures on silica surfaces and their adsorptive properties. *J Colloid Interface Sci*. 2005;285:18–26.
7. Auletta T, de Jong MR, Mulder A, van Veggel FCJM, Huskens J, Reinhoudt DN, Zou S, Zapotoczny S, Nherr HS, Vancso GJ, Kuipers L. β-Cyclodextrin host–guest complexes probed under thermodynamic equilibrium: thermodynamics and AFM force spectroscopy. *J Am Chem Soc*. 2004;126:1577–1584.
8. Endo H, Nakaji-Hirabayashi T, Morokoshi S, Gemmei-Ide M, Kitano H. Orientational effect of surface-confined cyclodextrin on the inclusion of bisphenols. *Langmuir*. 2005;21:1314–1321.

9. Sels BF, De Vos DE, Jacobs PA. Bromide-assisted oxidation of substituted phenols with hydrogen peroxide to the corresponding *p*-quinol and *p*-quinol ethers over WO_4^{2-}-exchanged layered double hydroxides. *Angew Chem Int Ed*. 2005;44:310–313.
10. Ogawa M, Kuroda K. Photofunctions of intercalation compounds. *Chem Rev*. 1995;95:399–438.
11. Liu ZP, Ma RZ, Osada M, Iyi N, Ebina Y, Takada K, Sasaki T. Synthesis, anion Exchange, and delamination of Co–Al layered double hydroxide: assembly of the exfoliated nanosheet/polyanion composite films and magneto-optical studies. *J Am Chem Soc*. 2006; 128:4872–4880.
12. Hu G, O'Hare D. Unique layered double hydroxide morphologies using reverse microemulsion synthesis. *J Am Chem Soc*. 2005;127: 17808–17813.
13. Newman SP, Jones W. Synthesis, characterization and applications of layered double hydroxides containing organic guests. *New J Chem*. 1998;22:105–115.
14. Zhao HT, Vance GF. Intercalation of carboxymethyl-β-cyclodextrin into magnesium-aluminum layered double hydroxide. *J Chem Soc, Dalton Trans*.1997:1961–1965.
15. Wang J, Wei M, Rao GY, Evans DG, Duan X. Structure and thermal decomposition of sulfated β-cyclodextrin intercalated in a layered double hydroxide. *J Solid State Chem*. 2004;177:366–371.
16. Bevinakatti HS, Banerji AA. Practical chemoenzymic synthesis of both enantiomers of propranolol. *J Org Chem*. 1991;56:5372–5375.
17. Lee LG, Whitesides GM. Preparation of optically active 1, 2-diols and α-hydroxy ketones using glycerol dehydrogenase as catalyst. Limits to enzyme-catalyzed synthesis due to noncompetitive and mixed inhibition by product. *J Org Chem*. 1986;51:25–36.
18. Iwasaki F, Maki T, Onomura O, Nakashima W, Matsumura Y. Chemo- and stereoselective monobenzoylation of 1, 2-diols catalyzed by organotin compounds. *J Org Chem*. 2000;65:996–1002.
19. Zhong QQ, Han XX, He LF, Beesley TE, Trahanovsky WS, Armstrong DW. Chromatographic evaluation of poly(*trans*-1,2-cyclohexanediyl-bisacrylamide) as a chiral stationary phase for HPLC. *J Chromatogr A*. 2005;1066:55–70.
20. Yuan LM, Xu ZG, Ai P, Chang YX, Azam AKMF. Effect of chiral additive on formation of cellulose triacetate chiral stationary phase in HPLC. *Anal Chim Acta*. 2005;554:152–155.
21. Galinada WA, Yoshida H. Intraparticle diffusion of phophates in OH-type strongly basic ion exchanger. *AICHE J*. 2004;50:2806–2815.
22. Yoshida H, Takastsuji W. Parallel transport of an organic acid by solid-phase and macropore diffusion in a weakly basic ion exchanger. *Ind Eng Chem Res*. 2000;39:1074–1079.
23. Yoshida H, Yoshikawa M, Kataoka T. Parallel transport of BSA by surface and pore diffusion in strongly basic chitosan. *AICHE J*. 1994;40:2034–2044.
24. Yoshida H, Kataoka T, Ikeda S. Intraparticle mass transfer in bidispersed porous ion exchanger. Part I: Isotopic ion exchange. *Can J Chem Eng*. 1985;63:422–429.
25. Yoshida H, Kataoka T. Intraparticle mass transfer in bidispersed porous ion exchanger. Part II: Mutual ion exchange. *Can J Chem Eng*. 1985;63:430–435.
26. Li P, Sengupta AK. Intraparticle diffusion during selective sorption of trace contaminants: the effect of gel versus macroporous morphology. *Environ Sci Technol*. 2000;34:5193–5200.
27. Maekawa M, Kasai K, Nango M. Transport phenomena of sulfonated dyes into cellulose membranes: parallel diffusion of a sulfonated dye with a high affinity onto cellulose. *Colloids Surfaces A: Physicochem Eng Aspects*. 1998;132:173–179.
28. Maekawa M, Ozeki S. Mixture diffusion of sulfonated dyes into cellulose membrane II. Effects of addition of a dye with lower affinity on parallel diffusion of a dye with high aggregation property. *Colloids Surfaces A: Physicochem Eng Aspects*. 1998;142: 99–105.
29. Crank J. *The Mathematics of Diffusion*. 2nd ed. Oxford, UK: Oxford Science Publications; 1975.
30. Hattori M, Okada Y, Takahashi K. Functional changes in β-lactoglobulin upon conjugation with carboxymethyl cyclodextrin. *J Agric Food Chem*. 2000;48:3789–3794.
31. Ravoo BJ, Darcy R, Mazzaglia A, Nolan D, Gaffney K. Supramolecular tapes formed by a catanionic cyclodextrin in water. *Chem Commun*. 2001;1:827–828.
32. Meyn M, Beneke K, Lagaly G. Anion-exchange reactions of layered double hydroxides. *Inorg Chem*. 1990;29:5201–5207.
33. Meyn M, Beneke K, Lagaly G. Anion-exchange reactions of hydroxy double salts. *Inorg Chem*. 1993;32:1209–1215.
34. Szejtli J. Introduction and general overview of cyclodextrin chemistry. *Chem Rev*. 1998;98:1743–1754.
35. Inacio J, Taviot-Gueho C, Forano C, Besse JP. Adsorption of MCPA pesticide by MgAl-layered double hydroxides. *Appl Clay Sci*. 2001;18:255–264.
36. Agrawal A, Sahu KK, Pandey BD. A comparative adsorption study of copper on various industrial solid wastes. *AICHE J*. 2004;50: 2430–2438.
37. Malek A, Farooq S. Kinetics of hydrocarbon adsorption on activated carbon and silica gel. *AICHE J*. 1997;43:761–776.
38. Giles GH, Mac Ewan TH, Nakhwa SN, Smith P. Studies in adsorption: Part XI. A system of classification of solution adsorption isotherms and its use in diagnosis of adsorption mechanisms and in measurement specific surface of solids. *J Chem Soc* 1960;3973–3993.

Manuscript received May 18, 2006, and revision received Mar. 9, 2007.